Title
Voltage tuning of vibrational mode energies in single-molecule junctions

Journal
Proceedings of the National Academy of Sciences of the United States of America, 111(4)

ISSN
0027-8424

Authors
Li, Yajing
Doak, Peter
Kronik, Leeor
et al.

Publication Date
2014-01-28

DOI
10.1073/pnas.1320210111

Peer reviewed

Voltage tuning of vibrational mode energies in single-molecule junctions

Yajing Li[a], **Peter Doak**[b,c], **Leeor Kronik**[d], **Jeffrey B. Neaton**[c,e,f], **and Douglas Natelson**[a,g,1]

[a]Department of Physics and Astronomy, Rice University, Houston, TX 77005; [b]Department of Chemistry, University of California, Berkeley, CA 94720; [c]Molecular Foundry, Lawrence Berkeley National Laboratory, Berkeley, CA 94720; [d]Department of Materials and Interfaces, Weizmann Institute of Science, Rehovoth 76100, Israel; [e]Department of Physics, University of California, Berkeley, CA 94720; [f]Kavli Energy Nanosciences Institute at Berkeley, Berkeley, CA 94720; and [g]Department of Electrical and Computer Engineering, Rice University, Houston, TX 77005

Edited by Abraham Nitzan, Tel Aviv University, Tel Aviv, Israel, and accepted by the Editorial Board December 21, 2013 (received for review October 25, 2013)

Vibrational modes of molecules are fundamental properties determined by intramolecular bonding, atomic masses, and molecular geometry, and often serve as important channels for dissipation in nanoscale processes. Although single-molecule junctions have been used to manipulate electronic structure and related functional properties of molecules, electrical control of vibrational mode energies has remained elusive. Here we use simultaneous transport and surface-enhanced Raman spectroscopy measurements to demonstrate large, reversible, voltage-driven shifts of vibrational mode energies of C_{60} molecules in gold junctions. C_{60} mode energies are found to vary approximately quadratically with bias, but in a manner inconsistent with a simple vibrational Stark effect. Our theoretical model instead suggests that the mode shifts are a signature of bias-driven addition of electronic charge to the molecule. These results imply that voltage-controlled tuning of vibrational modes is a general phenomenon at metal–molecule interfaces and is a means of achieving significant shifts in vibrational energies relative to a pure Stark effect.

plasmonics | nanoscale junctions | molecular electronics

Mechanical couplings between atoms within molecules, manifested through vibrational spectra, are critically important in many processes at the nanoscale, from energy dissipation to chemical reactions. These couplings originate from the self-consistent electronic structure and ionic positions within the molecule (1). Vibrational spectroscopy examines this bonding, and advanced time-resolved techniques (2–5) can manipulate vibrational populations. Single-molecule junctions (6, 7) also have proven to be valuable tools for examining vibrational physics. Previous work showed that vibrational frequencies may be altered in mechanical break junctions if the chemical linkage to the moving contacts is sufficient to strain bonds in the molecule (8, 9), but also showed vibrations to be unaffected when the linkage to the contacts is less robust (10). Controllably altering vibrational energies in the steady state is difficult, however. Electric fields can redistribute the molecular electron density and shift vibrational modes in the vibrational Stark effect (11), enabling spectroscopic probes of local static electric fields in charge double layers (12, 13) and biosystems (14–16). However, other physics also may be relevant, and studies of electrical tuning of molecular vibrational energies in single- or few-molecule–based solid-state junctions, which often provide clarity that is difficult to obtain from measurements of molecular ensembles, have been lacking.

Surface-enhanced Raman spectroscopy (SERS) (17, 18), in which surface plasmons enhance the Raman scattering rate for molecules, opens up the possibility of performing detailed vibrational studies at the single-molecule level. Plasmonic junctions between extended electrodes (19–25) show correlations of Raman response and conductance implying single- or few-molecule sensitivity, and enable studies of vibrational physics as a function of electrical bias. Spectral diffusion often is observed in single-molecule SERS experiments (18, 25, 26), and there is some preliminary evidence of bias-driven mode shifts in such junctions (23), with the mechanisms of these phenomena remaining unclear.

We report vibrational mode softening in C_{60} molecules on the order of tens of wavenumbers, approximately quadratic in the external dc bias, V, applied across such a junction. We compare these observations with density functional theory (DFT) calculations to determine the underlying mechanism. The calculations suggest that the systematic softening, its magnitude, and its detailed functional dependence on V are inconsistent with a pure vibrational Stark effect. Instead, changes in molecular charge with bias (27) result in vibrational shifts that closely resemble those observed in the experiments, both in magnitude and sign. This reveals a general physical mechanism, expected to have implications for other systems and measurements.

Fig. 1 shows a typical Raman spectrum from a C_{60}-containing junction, prepared by electromigration (28) of a lithographically defined Au constriction on an oxidized Si substrate. This junction is a useful test system, because C_{60} is known to adsorb sufficiently strongly to Au to allow the formation of reliable and reproducible junctions (29–31). The fabrication and detailed measurement procedures are discussed in *Materials and Methods*. The incident wavelength for the Raman measurements is 785 nm, and the extended electrode design allows the application of a dc bias, V, across the junction and the flow of current through it. The sharp mode at 520 cm^{-1} is from the Si substrate, and the modes between 1,000 cm^{-1} and 1,600 cm^{-1} are broadly consistent with expectations from previous C_{60} single-molecule SERS experiments and with our own calculations. We note that the close association of the molecule with the surface, necessary for SERS measurements, may result in chemical and symmetry changes that can turn previously Raman-inactive normal modes into active ones (32) and can lift mode degeneracies. Because each of our devices produces a unique Au junction possessing

Significance

Like guitar strings, molecules have characteristic vibrational frequencies, set by the strength of chemical bonding between the atoms. In an experiment using a special antenna for light, we have found that applying an electrical voltage to a single buckyball molecule systematically lowers its vibrational frequencies, indicating that the bonds are weakened. We can explain this observation in terms of a very simple, general model in which the applied voltage slightly increases the amount of negative charge on the molecule, thus tuning the chemical bond strength. This may be generally useful in understanding and controlling the mechanical properties of molecules.

Author contributions: D.N. designed research; Y.L., P.D., and J.B.N. performed research; Y.L., P.D., L.K., J.B.N., and D.N. analyzed data; and Y.L., P.D., L.K., J.B.N., and D.N. wrote the paper.

The authors declare no conflict of interest.

This article is a PNAS Direct Submission. A.N. is a guest editor invited by the Editorial Board.

[1]To whom correspondence should be addressed. E-mail: natelson@rice.edu.

This article contains supporting information online at www.pnas.org/lookup/suppl/doi:10.1073/pnas.1320210111/-/DCSupplemental.

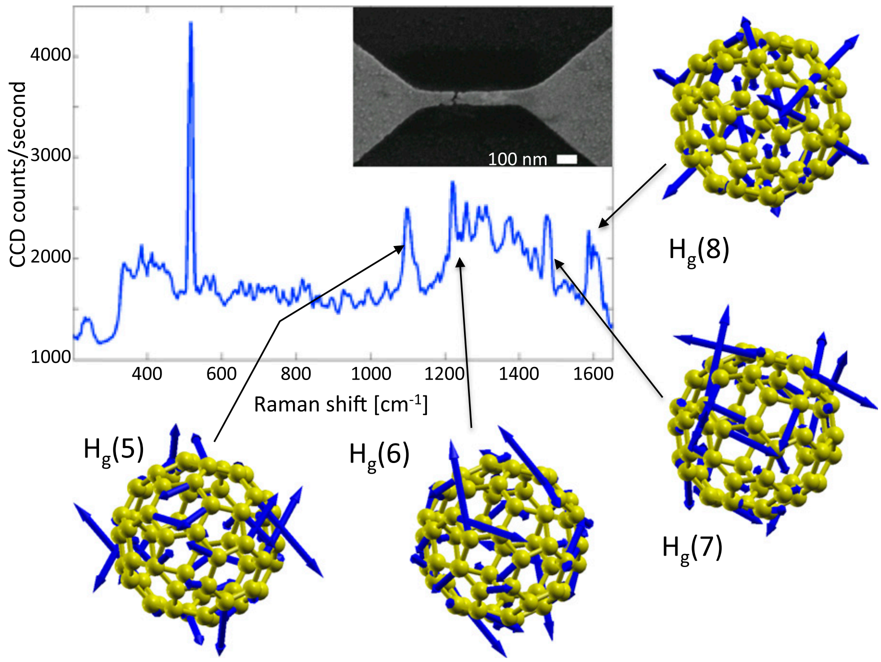

Fig. 1. Raman analysis of C_{60} in an electromigrated junction. (*Main Plot*) Example of a SERS spectrum of C_{60} in an electromigrated junction. Surrounding diagrams illustrate examples of the complicated displacements associated with Raman-active modes, calculated for an isolated, symmetric, gas-phase molecule. Each such mode is fivefold degenerate in the absence of symmetry breaking. (*Inset*) Scanning electron microscopic image of an electromigrated junction.

a specific molecular association, we track all normal modes of the molecules in the calculations. For the isolated C_{60} molecule, only the A_g and H_g modes are Raman active (they are labeled in Fig. 4*D*).

As in previous studies (20, 21, 23, 25, 33), correlations as a function of time are observed between spectral intensity fluctuations ("blinking") and the measured conductance in the tunneling regime. Because the tunneling conductance is dominated by a molecular-scale volume at the point of closest interelectrode separation, these correlations imply few- or single-molecule Raman sensitivity. For this study, the conductances range from 0.1 to a few $G_0 = 2e^2/h$ and include contributions from both through-molecule and direct metal–metal tunneling or contact in some junctions. These junctions are not in the Coulomb blockade regime.

Fig. 2 shows Stokes and anti-Stokes spectra as a function of applied bias for two representative devices. The main experimental observation is that many of the vibrational modes with energies greater than 1,000 cm^{-1} shift toward low energies as the applied bias increases. These systematic shifts are observed routinely in C_{60}-based junctions, having been seen in the 12 of 23 junctions that produced a significant and stable SERS signal. The remaining 11 junctions had blinking (junction configuration

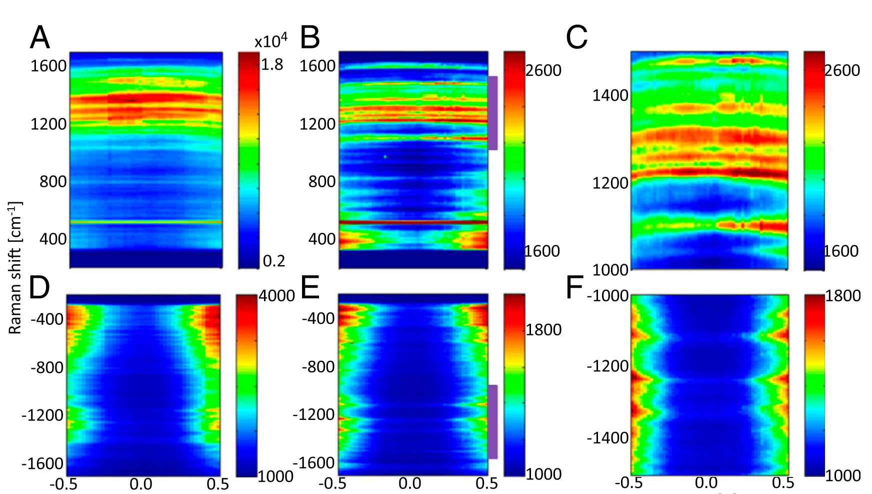

Fig. 2. Vibrational modes and their evolution with source-drain bias. (*A*) Stokes and (*D*) anti-Stokes spectra of device 1 as a function of *V*. (*B*) Stokes and (*E*) anti-Stokes spectra of device 2. Color scales indicate counts per integration time. (*C* and *F*) Rescaled close-ups of the device 2 data over the wavenumber ranges indicated by the purple bars in *B* and *E*, respectively. The vibrational modes curve slightly toward lower energies at larger $|V|$, and the anti-Stokes intensities increase at high biases. The latter effect indicates current-driven heating of vibrational degrees of freedom, as reported previously (22, 23). The spectral shifts are more difficult to resolve in the anti-Stokes case because of this evolution of anti-Stokes intensity.

instability) sufficiently strong that it precluded the long measurements required for a clear assessment of bias-driven effects. This yield and variation are consistent with prior experiments in such junctions.

The bias-driven shifts, apparent as a curvature of the spectral features, vary in magnitude, from a few centimeters^{-1} to 20 cm^{-1}. Fig. 3 shows data from another device, using a higher-resolution grating in the spectrometer. This particular dataset shows clear discontinuities in the mode intensities at a few bias voltages; these are stochastic blinking, as described above. The bias-driven shifts on the devices are consistent with a quadratic dependence on applied bias, $\delta\omega \sim V^2$. Note that electromigration junction experiments do not control the molecule/metal contact geometry precisely at the atomic scale; variability in the contact geometry and molecular environment may give junction-to-junction variations in the precise Raman spectrum. However, the sign, functional form, and magnitude of the bias-driven shifts here are consistent and reproducible.

To understand the mechanism at work, we use DFT to compute the vibrational frequencies of C_{60} as a function of external field and charge state. In principle, the local field and charge state of a molecule in a junction depend on atomistic features of the molecule–metal contact that are highly complex, are generally unknown, and vary from device to device. Here, we neglect explicit treatment of the electrodes and instead model the C_{60} environment, as a function of bias, through changes in fields and steady-state occupation. Initially, we compute the vibrational frequencies of a gas-phase C_{60} molecule in the presence of constant electric fields. For several external fields up to 1.2 V/nm (approximately twice the range probed by the experiment), the C_{60} geometry is relaxed and the vibrational modes are computed within DFT for constant charge state. Both neutral C_{60} and the $C_{60}{}^{-1}$ anion are considered. Mirjani et al. (34) recently considered the impact of full reduction or oxidation on vibrational modes of molecules in junctions, observing appreciable shifts relative to the neutral species. However, the lack of resonant transport (*Supporting Information*, Figs. S1–S3) confirms that the applied bias in this experiment is insufficient to fully change the average redox state of the molecule by an entire electron. Therefore, the anion represents the limit of charging possible in the system. For the neutral C_{60}, our calculations are in good agreement with previous theory and experiment (*Supporting Information*, Table S1). Calculated field-induced vibrational shifts for the neutral molecule (Fig. S4) (anion, Fig. S5) typically are far less than 1 cm^{-1} (5 cm^{-1}) in magnitude, at maximum field (1.2 V/nm); moreover, the shifts vary in sign and do not exhibit a generally quadratic functional form with field, in contrast to experiment. This rules out the well-known vibrational Stark effect as the origin of the observed phenomena.

A major clue toward an alternative explanation is that at constant field, differences between specific mode frequencies of the neutral and anion are large, of order 10–150 cm^{-1}, and notably, the affected anion modes are redshifted relative to the neutral molecule (*Supporting Information*). This suggests an explanation in terms of bias-driven changes of the C_{60} charge state. To explore this possibility, we recomputed the C_{60} vibrational spectrum, adding small fractions of an electron, from 0 to 1, in steps of 0.1 *e*. In the case of significant hybridization between the molecule and metal contact, partially occupied states in the junction are expected. Furthermore, in an open system, a fractional number of electrons in DFT is defined via an ensemble of integer-electron states and interpreted as a time average of a fluctuating number of particles (35). Therefore, one may infer the effect of partial molecular charging in the junction from calculations of a single partially charged C_{60} molecule. A fractional

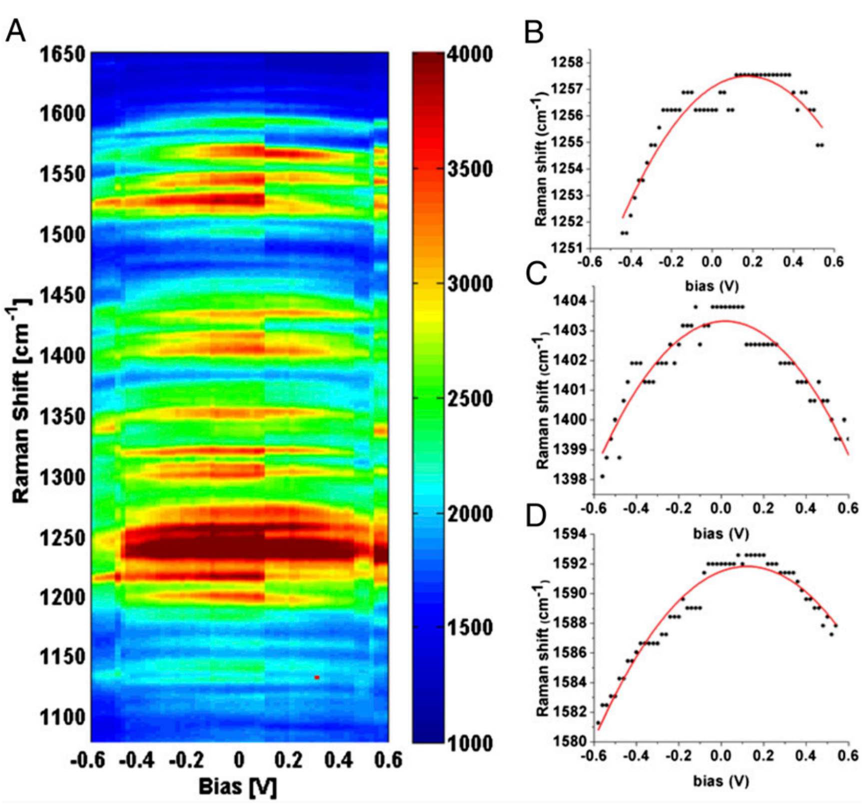

Fig. 3. Bias-driven vibrational energy shifts. (*A*) Raman response of device 3 as a function of bias (*x* axis) and Raman shift (*y* axis). The sudden change in the intensity at around 0.1 V is the result of blinking. (*B–D*) Vibrational energy shift as a function of bias for three particular modes: 1,258 cm^{-1}, 1,404 cm^{-1}, and 1,592 cm^{-1}. The discretized Raman shift data result from pixilation of the detector.

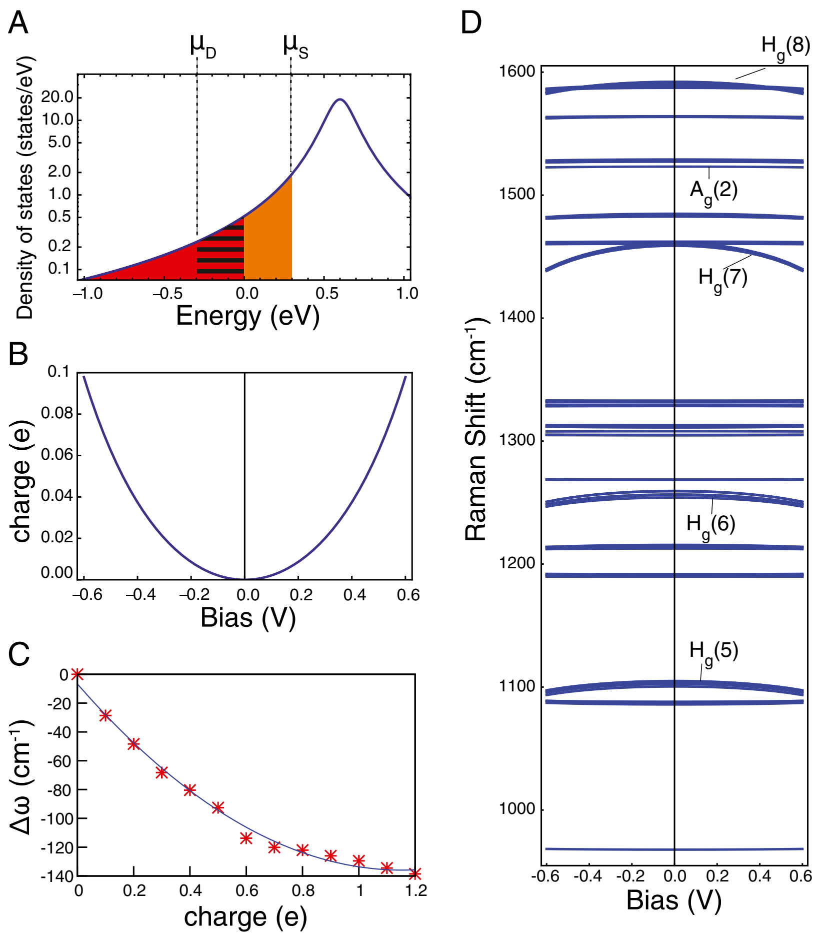

Fig. 4. Model of bias-driven changes in molecular charging. (*A*) At zero bias, the triply degenerate LUMO resonance, centered at E_0 with width Γ, is occupied proportionally by the red shading. As the bias *V* is applied, the molecular level gains additional occupation proportional to the area shown by the orange shading and loses occupation proportional to the hatched portion of the Lorentzian. (*B*) The expression for charging with bias at 80 K (solid) is visually identical to the charging at 0 K (for 300-K charging, see *Supporting Information*). The change in partial charge is approximately quadratic in bias. (*C*) A representative mode's [Hg(7) at 1,467 cm^{-1}] change in vibrational energy with charging, computed via DFT. This dependence, combined with the variation in charge with bias, strongly suggests that bias-driven charging is the origin of the systematic mode softening observed in the experiments. (*D*) Mode energies as a function of bias from such a calculation.

occupation of the C_{60} lowest unoccupied molecular orbital (LUMO) upon adsorption into a junction is consistent with the established large electronegativity of C_{60} (29, 36) and with scanning tunneling microscopy (STM) studies of C_{60} adsorbed on clean metal surfaces (37). As the molecule is (partially) charged, several C_{60} vibrational modes shift systematically to lower energies, by tens of centimeters^{-1} (Fig. S6). We compute that these are Raman-active H_g modes* that couple strongly to the t_{1u} LUMO (38–42) and are present throughout the 1,000–1,600-cm^{-1} measurement range (Fig. 4). This trend is reasonable on general chemistry grounds: Adding an electron to the neutral C_{60} occupies an antibonding LUMO that is delocalized over the entire molecule, thereby softening many intramolecular bonds. Thus, a redshift of vibrational modes coupled to an antibonding LUMO upon electronic charging would be expected quite generally.

Only a relatively small amount of charging is necessary to result in the mode shifts seen here, and small changes in charge state are very plausible under bias. Fig. 4 shows a simple model for the energy level alignment of the junction. At zero applied bias, the triply degenerate LUMO resonance will be positioned near the Fermi energy (37, 43), and broadened by its coupling to the source and drain electrodes. Assuming that electrons tunneling from the source to drain and drain to source, respectively; that they are noninteracting and therefore are occupied according to their original source or drain quasi-Fermi levels (44); and that the resonance line shape is Lorentzian with a width $\Gamma = \Gamma_S + \Gamma_D$, the change in steady-state occupation, δρ, of a single triply degenerate level at energy E_0 above the equilibrium Fermi level E_F, at bias V, may be expressed as (1, 27)

$$\delta\rho = \int_{-\infty}^{\infty} {}^{1}\!/_{2}\, g(E)\left[f\left(E+{}^{eV}\!/_{2}\right)+f\left(E-{}^{eV}\!/_{2}\right)-2f(E)\right]dE,$$

where, in this case, the density of states $g(E) = (d\,\Gamma/\pi)/(\Gamma^2 + (E - E_0)^2)$ is Lorentzian with degeneracy d ($d = 6$ in this case because of spin and orbital degeneracy) and $f(E) = 1/(e^{E/kT} + 1)$ is the Fermi–Dirac distribution function, with the zero-bias Fermi level E_F taken as the energy reference, i.e., $E_F = 0$. Here a symmetrical voltage drop is assumed, with the source and drain chemical potentials taken to be $\mu_S = eV/2$ and $\mu_D = -eV/2$, respectively. Recently, Kaasbjerg et al. (45) developed a nonequilibrium Green

*A_g modes also couple to the t_{1u} LUMO, but because the symmetric A_g modes do not break the LUMO degeneracy and therefore are not involved in the Jahn–Teller distortion (38–42), they vary less significantly with bias.

function framework for understanding bias-dependent molecular vibrational mode damping and heating in junctions. Including physics similar to what we consider here with our C_{60}-specific model, this approach also captures vibrational frequency renormalization associated with charging and screening (45), and is consistent with the work presented here in the limit where Γ is small compared with the resonance energy and bias voltage.

Previous STM experiments and DFT calculations of C_{60} on metal surfaces yielded $\Gamma \sim 0.1$ eV and $E_0 \sim 1.0$ eV (43). However, in a junction environment, where C_{60} is contacted on both sides with rough surfaces, E_0 will be closer to E_F (37). Depending on the specifics of the Au–C_{60} contact within a particular junction, E_0 may vary somewhat. The value for Γ also will vary to some degree, but numerous experiments have shown significant coupling of C_{60} to Au. To demonstrate our reasoning, we take $E_0 = 0.6$ eV above E_F at zero bias and $\Gamma = 0.1$ eV. (The effect of finite temperature is shown in Fig. S7, and the effect of other choices for these parameters is explored in Fig. S8, but the general effect of charging is preserved). Together with the above model dependence of $\delta\rho$ on V (Fig. 4*B*) and DFT-computed dependence of the frequency on $\delta\rho$ (Fig. 4*C*), we compute the vibrational mode frequency as a function of bias for voltages up to ±0.6 V, as shown in Fig. 4*D*. This simple model explains the measured mode softening trends.

For the choice of model parameters E_0 and Γ, the finite temperature spread of the Fermi–Dirac distribution of the electrons in the source and drain has a negligible effect on the molecular charge at 80 K, but is more important at 300 K (Fig. S7). This suggests that any heating of the electronic distribution at high bias (23) also might play a role in determining the molecular charge and, hence, vibrational energies.

Using nanojunction-based SERS, we observe systematic bias-driven softening of vibrational modes in C_{60}. Comparisons with DFT calculations show that Stark physics alone cannot be responsible for these effects, and bias-driven alteration of the molecular charge state is the likely explanation. By combining realistic computational models of junctions with measurements of this type, the presence and degree of bias-induced mode softening can turn these junctions into a direct local probe of molecule/metal energetics. Interpreted in light of these observations, the earlier preliminary observations of bias-driven mode softening in a junction based on an oligo(phenylene vinylene) (OPV) molecule (23) suggest that in that particular device, the LUMO must lie close to the electrode Fermi levels. Indeed, recent calculations by Kaasbjerg et al. (45) arrive at similar conclusions regarding the origin of OPV mode shifts under bias observed in ref. 5. Similarly, it is worth considering whether much of the spectral diffusion observed in single-molecule Raman measurements results from small changes in the effective molecular charge density, changes in the occupation of proximal surface states, or the presence/absence of nearby molecular adsorbates. Finally, the observations reported here point out that considerable care should be taken in the interpretation of vibrational Stark effect data in other contexts. Although good agreement between theoretical expectations and observations has been reported (11), when considering only Stark physics, it is important to note that charging effects may be of similar or greater magnitudes in some circumstances.

Materials and Methods

The SERS substrates for the measurements are produced by electromigration of lithographically defined metal constrictions fabricated on underlying oxidized Si substrates. The bowtie structures are patterned by electron beam lithography. The constriction of the bowtie structure is 100–120 nm wide and 1 μm long, as shown in Fig. 1, *Inset*. Evaporation of 1 nm Ti and 15 nm Au onto the bowtie structure is followed by lift-off in acetone. The larger, extended contact pads for the bowtie structure are evaporated with 1 nm Ti and 30 nm gold by using a shadow mask. The substrates are cleaned by oxygen plasma for 2 min to remove organic contamination and then spin coated with a solution of C_{60} at a concentration of 1 mg of C_{60} per 10 mL toluene. The C_{60} molecules undergo physisorption directly on the electrode surfaces, with no linker groups or linker chemistry. The chips are wire-bonded to a ceramic carrier and placed within a microscope cryostat. Once cooled to 80 K under a vacuum of 6×10^{-6} milliBar, each junction is electromigrated through a computer-controlled procedure to yield interelectrode tunneling conductances near or below $G_0 = 2e^2/h$.

Raman spectroscopy is performed using a home-built Raman microscope system, with an incident wavelength of 785 nm. Modes with Stokes or anti-Stokes shifts below 300 cm^{-1} are cut off by a notch filter. A piezo-actuated lens mount rasters the diffraction-limited beam over the sample surface, allowing the acquisition of spatially mapped Raman response. The mapped Si Raman intensity at 520 cm^{-1} is used to locate the center of a bowtie structure. Following electromigration, another Raman image determines the location of the nanogap's plasmonic Raman hotspot. Raman spectra at that location then are acquired simultaneously with electronic transport data (I and dI/dV as a function of V, using a current preamplifier; V sourced by a digital-to-analog converter integrated into a lock-in amplifier; and differential conductance measured via lock-in using a 10-mV ac signal added to V with a summing amplifier). Fig. 1 is an example of a single surface-enhanced Raman spectrum of such a junction, acquired with a 1-s integration time. The sharp mode at 520 cm^{-1} is from the underlying Si substrate, and the modes between 1,000 cm^{-1} and 1,600 cm^{-1} agree reasonably well with expectations from other SERS studies of C_{60}. Transport data acquisition was synchronized with spectral measurements through triggering. The bias, V, was swept from −0.5 V to 0.5 V in steps of 0.0125 V or 0.025 V. The acquisition time for each spectrum at every voltage was 1–3 s. A higher-resolution grating is available for detailed studies, although this grating precludes simultaneous measurements of both Stokes and anti-Stokes emission.

All calculations were performed using the Siesta 3.1 code (46), using the generalized gradient exchange-correlation functional of Perdew, Burke, and Ernzerhof (PBE) (47). The C pseudopotential used a core radius cutoff of 1.29 bohr for 2*s*, 2*p*, and 2*d* channels. A triple zeta basis set was used for 2*s* and 2*p* functions, with a single zeta 2*d* polarization function. All calculations were performed with a 1000 Rydberg real space grid and 30 × 30 × 30-Å supercells. All structures at all charges and fields were relaxed until forces were less than 0.004 eV/Å. Vibrations were calculated using Siesta's Vibra package (48).

ACKNOWLEDGMENTS. Y.L. and D.N. acknowledge support from Robert A. Welch Foundation Grant C-1636. Work by P.D. and J.B.N. was supported by the US Department of Energy, Office of Basic Energy Sciences, Materials Sciences and Engineering Division, under Contract DE-AC02-05CH11231. Portions of this work at the Molecular Foundry were supported by the Office of Science, Office of Basic Energy Sciences, of the US Department of Energy under the same contract. Computational resources were provided by the National Energy Research Scientific Computing Center. Work by L.K. was supported by the Israel Science Foundation and the Lise Meitner Center for Computational Chemistry.

1. Nitzan A (2006) *Chemical Dynamics in Condensed Phases: Relaxation, Transfer and Reactions in Condensed Molecular Systems: Relaxation, Transfer and Reactions in Condensed Molecular Systems* (Oxford Univ Press, Oxford).
2. Brinks D, et al. (2010) Visualizing and controlling vibrational wave packets of single molecules. *Nature* 465(7300):905–908.
3. Evans CL, Xie XS (2008) Coherent anti-stokes Raman scattering microscopy: Chemical imaging for biology and medicine. *Annu Rev Anal Chem (Palo Alto Calif)* 1:883–909.
4. Hochstrasser RM (2007) Two-dimensional spectroscopy at infrared and optical frequencies. *Proc Natl Acad Sci USA* 104(36):14190–14196.
5. Zheng JR, et al. (2005) Ultrafast dynamics of solute-solvent complexation observed at thermal equilibrium in real time. *Science* 309(5739):1338–1343.
6. Aradhya SV, Venkataraman L (2013) Single-molecule junctions beyond electronic transport. *Nat Nanotechnol* 8(6):399–410.
7. Song H, Reed MA, Lee T (2011) Single molecule electronic devices. *Adv Mater* 23(14): 1583–1608.
8. Djukic D, et al. (2005) Stretching dependence of the vibration modes of a single-molecule Pt-H_2-Pt bridge. *Phys Rev B* 71(16):161402.
9. Arroyo CR, et al. (2010) Characterization of single-molecule pentanedithiol junctions by inelastic electron tunneling spectroscopy and first-principles calculations. *Phys Rev B* 81(7):075405.
10. Kiguchi M, et al. (2008) Highly conductive molecular junctions based on direct binding of benzene to platinum electrodes. *Phys Rev Lett* 101(4):046801.

11. Boxer SG (2009) Stark realities. *J Phys Chem B* 113(10):2972–2983.
12. Lambert DK (1988) Vibrational Stark-effect of Co on Ni(100), and Co in the aqueous double-layer—experiment, theory, and models. *J Chem Phys* 89(6):3847–3860.
13. Oklejas V, Sjostrom C, Harris JM (2003) Surface-enhanced Raman scattering based vibrational Stark effect as a spatial probe of interfacial electric fields in the diffuse double layer. *J Phys Chem B* 107(31):7788–7794.
14. Suydam IT, Snow CD, Pande VS, Boxer SG (2006) Electric fields at the active site of an enzyme: Direct comparison of experiment with theory. *Science* 313(5784):200–204.
15. Hu WH, Webb LJ (2011) Direct measurement of the membrane dipole field in bicelles using vibrational Stark effect spectroscopy. *J Phys Chem Lett* 2(15):1925–1930.
16. Schkolnik G, et al. (2012) Mapping local electric fields in proteins at biomimetic interfaces. *Chem Commun (Camb)* 48(1):70–72.
17. Kneipp K, et al. (1997) Single molecule detection using surface-enhanced Raman scattering (SERS). *Phys Rev Lett* 78(9):1667–1670.
18. Nie SM, Emory SR (1997) Probing single molecules and single nanoparticles by surface-enhanced Raman scattering. *Science* 275(5303):1102–1106.
19. Ioffe Z, et al. (2008) Detection of heating in current-carrying molecular junctions by Raman scattering. *Nat Nanotechnol* 3(12):727–732.
20. Konishi T, et al. (2013) Single molecule dynamics at a mechanically controllable break junction in solution at room temperature. *J Am Chem Soc* 135(3):1009–1014.
21. Liu Z, et al. (2011) Revealing the molecular structure of single-molecule junctions in different conductance states by fishing-mode tip-enhanced Raman spectroscopy. *Nat Commun* 2:305.
22. Natelson D, Li YJ, Herzog JB (2013) Nanogap structures: Combining enhanced Raman spectroscopy and electronic transport. *Phys Chem Chem Phys* 15(15):5262–5275.
23. Ward DR, Corley DA, Tour JM, Natelson D (2011) Vibrational and electronic heating in nanoscale junctions. *Nat Nanotechnol* 6(1):33–38.
24. Ward DR, et al. (2007) Electromigrated nanoscale gaps for surface-enhanced Raman spectroscopy. *Nano Lett* 7(5):1396–1400.
25. Ward DR, et al. (2008) Simultaneous measurements of electronic conduction and Raman response in molecular junctions. *Nano Lett* 8(3):919–924.
26. Emory SR, Jensen RA, Wenda T, Han MY, Nie SM (2006) Re-examining the origins of spectral blinking in single-molecule and single-nanoparticle SERS. *Faraday Discuss* 132:249–259, discussion 309–319.
27. Darancet P, Widawsky JR, Choi HJ, Venkataraman L, Neaton JB (2012) Quantitative current-voltage characteristics in molecular junctions from first principles. *Nano Lett* 12(12):6250–6254.
28. Park H, Lim AKL, Alivisatos AP, Park J, McEuen PL (1999) Fabrication of metallic electrodes with nanometer separation by electromigration. *Appl Phys Lett* 75(2): 301–303.
29. Lu XH, Grobis M, Khoo KH, Louie SG, Crommie MF (2003) Spatially mapping the spectral density of a single C60 molecule. *Phys Rev Lett* 90(9):096802.
30. Yee SK, Malen JA, Majumdar A, Segalman RA (2011) Thermoelectricity in fullerene-metal heterojunctions. *Nano Lett* 11(10):4089–4094.
31. Lörtscher E, et al. (2013) Bonding and electronic transport properties of fullerene and fullerene derivatives in break-junction geometries. *Small* 9(2):209–214.
32. Lund PA, Smardzewski RR, Tevault DE (1982) Surface-enhanced Raman spectra of benzene and benzene-d6 on vapor-deposited sodium. *Chem Phys Lett* 89(6):508–510.
33. Sonntag MD, Chulhai D, Seideman T, Jensen L, Van Duyne RP (2013) The origin of relative intensity fluctuations in single-molecule tip-enhanced Raman spectroscopy. *J Am Chem Soc* 135(45):17187–17192.
34. Mirjani F, Thijssen JM, Ratner MA (2012) Probing charge states in molecular junctions using Raman spectroscopy. *J Phys Chem C* 116(43):23120–23129.
35. Perdew JP, Parr RG, Levy M, Balduz JL (1982) Density-functional theory for fractional particle number—derivative discontinuities of the energy. *Phys Rev Lett* 49(23): 1691–1694.
36. Sau JD, Neaton JB, Choi HJ, Louie SG, Cohen ML (2008) Electronic energy levels of weakly coupled nanostructures: C60-metal interfaces. *Phys Rev Lett* 101(2):026804.
37. Bilan S, Zotti LA, Pauly F, Cuevas JC (2012) Theoretical study of the charge transport through C-60-based single-molecule junctions. *Phys Rev B* 85(20):205403.
38. Ramanantoanina H, Gruden-Pavlovic M, Zlatar M, Daul C (2013) Density functional theory study of the multimode Jahn-Teller problem in the fullerene anion. *Int J Quantum Chem* 113(6):802–807.
39. Alqannas HS, Lakin AJ, Farrow JA, Dunn JL (2013) Interplay between Coulomb and Jahn-Teller effects in icosahedral systems with triplet electronic states coupled to h-type vibrations. *Phys Rev B* 88(16):165430.
40. Laflamme Janssen J, Côté M, Louie SG, Cohen ML (2010) Electron-phonon coupling in C_{60} using hybrid functionals. *Phys Rev B* 81(7):073106.
41. Varma CM, Zaanen J, Raghavachari K (1991) Superconductivity in the fullerenes. *Science* 254(5034):989–992.
42. Haddon RC, Brus LE, Raghavachari K (1986) Electronic-structure and bonding in icosahedral C-60. *Chem Phys Lett* 125(5-6):459–464.
43. Lu XH, Grobis M, Khoo KH, Louie SG, Crommie MF (2004) Charge transfer and screening in individual C-60 molecules on metal substrates: A scanning tunneling spectroscopy and theoretical study. *Phys Rev B* 70(11):115418.
44. Di Ventra M (2008) *Electrical Transport in Nanoscale Systems* (Cambridge Univ Press, Cambridge, UK).
45. Kaasbjerg K, Novotný T, Nitzan A (2013) Charge-carrier-induced frequency renormalization, damping and heating of vibrational modes in nanoscale junctions. *Phys Rev B* 88(20):201405(R).
46. Soler JM, et al. (2002) The SIESTA method for ab initio order-N materials simulation. *J Phys Condens Matter* 14(11):2745–2779.
47. Perdew JP, Burke K, Ernzerhof M (1996) Generalized gradient approximation made simple. *Phys Rev Lett* 77(18):3865–3868.
48. Artacho E, et al. (2008) The SIESTA method; developments and applicability. *J Phys Condens Matter* 20(6):064208.